Composites: Part A 190 (2025) 108652

Contents lists available at ScienceDirect

Composites Part A

journal homepage: www.elsevier.com/locate/compositesa

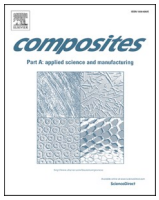

High-performance automotive adhesives with urethane-modified and nanophase-separated epoxy systems

Kyeng-Bo Sim [a], Jong-Ho Back [a,b], Gi-Yeon Han [a], Hyun-Joong Kim [a,b,*]

[a] Program in Environmental Materials Science, Department of Agriculture, Forestry and Bioresources, Seoul National University, Seoul 08826, Republic of Korea
[b] Research Institute of Agriculture and Life Sciences, College of Agriculture and Life Sciences, Seoul National University, Seoul 08826, Republic of Korea

ARTICLE INFO

Keywords:
Epoxy resins
Energy absorption
Impact strength
Phase separation
Automotive adhesives

ABSTRACT

Epoxy resins are extensively used across various industries due to their exceptional adhesive strength, mechanical properties, and chemical resistance. However, their inherent brittleness, low crack resistance, and limited elongation and fracture toughness restrict their standalone applications. Although numerous toughening strategies have been explored, challenges such as increased viscosity, difficulties in achieving uniform dispersion, opacity, and limited improvement in elongation remain unresolved. To address these limitations, aliphatic diols with urethane linkages were synthesized with varying diamine chain lengths (230, 400) and used as additives in epoxy systems, resulting in the formation of nano-sized domains that promote phase separation. This phase-separated structure facilitated uniform stress distribution and enhanced energy absorption, leading to an elongation of 11.5 % at 50 % A-D230. A-D400 formed larger domains, exhibiting superior performance under high impact, with an Izod impact strength of 72 J/m. Furthermore, aliphatic-modified epoxy synthesized through the thermal reaction of aliphatic diol with epichlorohydrin, when used as a reactant, acted as a flexible segment in the epoxy matrix, enhancing stress absorption and toughness. This approach also demonstrated improved thermal stability and shear strength. The toughening strategies utilizing additives and reactants in epoxy can be tailored to meet the specific performance requirements, such as adhesive strength, impact resistance, durability, and fatigue life, making these epoxy systems highly applicable for automotive adhesive formulations.

1. Introduction

Epoxy resins are widely used thermosetting materials, valued for their mechanical and chemical stability, heat resistance, corrosion resistance, electrical insulation, and strong adhesive properties. These properties make epoxy resins essential for high-performance applications in industries such as aerospace, automotive, electronics, and semiconductor packaging [1–4]. However, the highly cross-linked structure of epoxy resins results in inherent brittleness, reduced fracture toughness, and limited elongation, restricting their use in more demanding environments [5–7].

Therefore, epoxy resins are often reinforced using various toughening methods instead of being used alone [8–12]. Traditional toughening approaches include the incorporation of rubber-based modifiers [13–15], core–shell polymers [16,17], and nanoparticles [18–20], which are highly effective in enhancing impact strength and toughness. However, these methods are often associated with challenges such as increased viscosity, difficulties in achieving uniform dispersion [21–23], and reduced transparency [24]. Furthermore, while toughness may improve, elongation enhancement remains limited, restricting the use of epoxy resins in applications requiring high flexibility and durability [25–27].

To overcome these limitations, we introduced aliphatic diols with urethane linkages as additives to develop a novel epoxy toughening strategy. These low-molecular-weight diols form nano-scale domains within the epoxy matrix, which address critical challenges associated with conventional epoxy toughening agents. Specifically, they mitigate issues related to viscosity increase, ensure uniform dispersion, maintain transparency, and exhibit high compatibility with the polymer matrix. This unique approach is expected to overcome the limitations of existing toughening materials. Additionally, while impact resistance is typically improved at the expense of reduced elongation due to the inherent trade-off relationship, the design of this heterogeneous structure aims to minimize this trade-off effectively.

* Corresponding author.
E-mail address: hjokim@snu.ac.kr (H.-J. Kim).

https://doi.org/10.1016/j.compositesa.2024.108652
Received 2 October 2024; Received in revised form 29 November 2024; Accepted 9 December 2024
Available online 24 December 2024

Phase separation mechanisms can be broadly categorized into reaction-induced phase separation and pre-cure phase-separated retention. Reaction-induced phase separation occurs during the curing process, driven by chemical reactions and changes in interactions among the components [28–31]. In contrast, pre-cure phase-separated retention occurs when phase separation is already established before curing and remains fixed after the curing process [3]. The phase separation mechanism observed in this study corresponds to pre-cure phase-separated retention. Specifically, thermoplastic diols with molecular weights of 230 and 400 were employed as inert fillers, which do not chemically react with the epoxy matrix during curing. Due to their inherent immiscibility with the epoxy resin, these diols form a phase-separated morphology before curing. As curing progresses, the epoxy matrix solidifies, preserving the dispersed state of the thermoplastic diols and locking the phase-separated structure in place.

This retained phase-separated structure plays a critical role in enhancing material properties such as stress relaxation, elongation, and impact resistance. The thermoplastic domains facilitate energy absorption and stress redistribution, significantly improving ductility and impact resistance. Furthermore, the optimized stress distribution and energy absorption are expected to enhance long-term reliability under fatigue conditions.

To address the limitations associated with additive-based toughening, such as reduced crosslinking density, diminished thermal stability, and weakened adhesive performance due to phase separation, we developed a urethane-modified epoxy system by thermally reacting aliphatic diols with epichlorohydrin. This urethane-modified epoxy, when used as a reactant, forms flexible segments uniformly within the epoxy matrix, enhancing stress absorption and mechanical strength. Furthermore, it improves both thermal stability and shear strength, making it highly advantageous in demanding applications. This study demonstrates how the combined use of phase separation and urethane modification can overcome the drawbacks of traditional epoxy toughening strategies, offering tailored enhancements in both mechanical and thermal performance.

2. Materials and methods

2.1. Materials

Jeffamine D-230 (Mw = 230 g/mol, Huntsman), Jeffamine D-400 (Mw = 430 g/mol, Huntsman), propylene carbonate (PC, 98 %, Sigma-Aldrich), epichlorohydrin (Sigma-Aldrich), anhydrous magnesium sulfate ($MgSO_4$, Samchun Chemical), and tetrabutylammonium bromide (Alfa Aesar) were used as supplied without further purification. Sodium hydroxide and dichloromethane (DCM, 99.8 %) were purchased from Samchun Chemicals.

2.2. Aliphatic diol (A-D230, A-D400)

A 500-mL flask was charged with propylene carbonate and Jeffamine D-230 or D-400 in molar ratios of 1:1 and 1:2, respectively. The reaction mixture was mechanically stirred at 100 °C for 4 d for A-D230 and 5 d for A-D400 under ambient conditions. After the reaction, the mixture was diluted with 1 L of water and 1 L of dichloromethane (DCM), followed by five extractions with water. The DCM phase containing the product was separated, and any residual water was removed using anhydrous magnesium sulfate ($MgSO_4$). The final solution was dried in a vacuum oven for 3 d. Details about the content can be found in Table 1 and Table S1.

2.3. Urethane modified epoxy (Reactant U-230, U-400)

A 100-mL vessel was charged with A-D230 or A-D400, sodium hydroxide pellets, and epichlorohydrin. The mixture was stirred at room temperature for 30 min. Tetrabutylammonium bromide was then added as a catalyst, and the reaction was allowed to proceed at 50 °C for 3 h. After the reaction, the resulting brown-colored product and residual solids were filtered out. To remove any residual monomers, the filtrate was diluted with water and dichloromethane, following the same procedure as that for A-D230 and A-D400 preparation. The solution was then dried using anhydrous magnesium sulfate, and the final product was placed in a vacuum oven for 3 d to ensure complete drying. Details about the content can be found in Table 1 and Table S1.

Table 1
Components of adhesives.

Material	Composition	Equivalent (g/eq)	Form
DGEBA	Bisphenol A diglycidyl ether	187	Liquid
R-UME230	Aliphatic urethane modified epoxy	273.1	Liquid
R-UME400	Aliphatic urethane modified epoxy	410.2	Liquid
A-Diol230	Aliphatic diol		Liquid
A-Diol400	Aliphatic diol		Liquid
IPDA	Isophorone diamine	42.6	Liquid

For the A-D230 and A-D400 aliphatic diols, the equivalent ratio (stoichiometry) was not considered, as they do not react directly with the curing agent. However, for diglycidyl ether bisphenol A (DGEBA, Kukdo Chemical, EEW = 184–190 g/eq) and the urethane-modified epoxies R-U230 (EEW = 273.145 g/eq) and R-U400 (EEW = 410.15 g/eq), the curing agent used was isophorone diamine (IPDA, Sigma-Aldrich, EEW = 42.58 g/eq), and the resin-to-curing agent ratio was calculated as 1:1 based on their equivalent weights. For the preparation of the blends, A-D230 and A-D400 were mixed with epoxy in varying proportions of 0, 10, 20, 30, 40, and 50 wt%, followed by curing at 115 °C. For R-U230 and R-U400, they were also mixed with epoxy at the same content levels (0, 10, 20, 30, 40, and 50 wt%), and the combined equivalent weights of the epoxy and urethane-modified epoxy were used to calculate the 1:1 ratio with the curing agent. The curing for R-U230 and R-U400 was carried out at 125 °C. The curing temperature was determined using differential scanning calorimetry (DSC), with the top peak used as the reference point for setting the curing temperature.

2.4. Small angle X-ray scattering (SAXS)

SAXS data was collected using a XEUSS 2.0 instrument equipped with a Pilatus 300 K detector (Dectris). The sample-to-detector distance, wavelength, and sample thickness were set at 1000 mm, 1.542 Å, and 60 μm, respectively. The scattering vector (q) was calculated from the scattering angle (2θ) using the formula: $q = (4\pi/\lambda)\sin\theta$.

2.5. Solvent dissolution

The synthesized DGEBA, A-D230, A-D400, R-U230, and R-U400 samples were placed in conical tubes and immersed in the solvent dichloromethane (DCM). The tubes were shaken at 50 rpm for 2 d. The weight loss was measured relative to the initial weight, and the percentage of weight loss was calculated using the following formula:

$$Weightloss(\%) = \frac{W_{initial} - W_{final}}{W_{initial}} \times 100$$

2.6. Field emission scanning electron microscopy (FE-SEM)

Field emission scanning electron microscopy (FE-SEM; SUPRA 55VP, Carl Zeiss, Germany) was used to observe the surface morphology of the samples after solvent dissolution. FE-SEM analysis was employed to examine the formation of phase separation based on the content and chain length of the samples. Additionally, the fracture surfaces after the Izod impact test were analyzed to observe the failure patterns and fracture mechanisms post-impact.

2.7. Dynamic mechanical analysis (DMA)

Dynamic mechanical analysis (DMA) was conducted using a Q800 dynamic mechanical analyzer (TA Instruments) in the dual cantilever mode, operating at an oscillation frequency of 1 Hz with a strain amplitude of 0.1 %. The temperature was varied from 20 °C to 200 °C at a heating rate of 5 °C/min. The glass transition temperature (Tg) was determined from the tan δ versus temperature curve. Additionally, DMA was used to measure the storage modulus, loss modulus, and Tg and to calculate the crosslinking density, which provided insights into the mechanical and thermal properties of the materials.

2.7.1. Crosslinking density

The crosslinking density (ν_c) of the cured epoxy resins A-D230, A-D400, R-U230, and R-U400 wt% was calculated using the equation. In this equation, R represents the gas constant, T is the absolute temperature at Tg + 50 °C + 273.15°C, and E'_e represents the storage modulus measured at Tg + 50 °C.

$$\nu_c = \frac{E'_e}{3RT}$$

2.8. Izod impact test

The Izod impact test specimens were prepared using rectangular steel molds with dimensions of 80 mm (length) × 10 mm (width) × 4 mm (thickness). A 2-mm deep notch was placed at the center of each specimen. The impact strength was determined by measuring the absorbed energy per unit width under impact conditions. The test had a capacity of 750 J·m^{-1}. Five specimens from each sample were tested at a temperature of 23 °C.

2.9. Tensile test

Tensile test specimens were prepared using dumbbell-shaped steel molds in accordance with ISO 527–2, with the DGEBA, A-D230, A-D400, R-U230, and R-U400 samples prepared according to their respective wt % contents. A Universal Testing Machine (UTM, model 5982, Instron) was used at a constant strain rate of 5 mm/min. For the phase-separated samples, additional tensile tests were conducted at varying strain rates (1, 5, 10, 20, 40, and 80 mm/min) to assess their behavior under different testing speeds. The tensile strength and strain at break were defined as the maximum stress and elongation at the point of fracture, respectively. The tests were performed at room temperature (23 °C) and were repeated five times to ensure accuracy.

2.10. Single-lap shear test

Epoxy resin was applied to a steel substrate (type: CR340, length: 100 mm, width: 25 mm, thickness: 1.6 mm) over an adhesion area of 12.5 mm × 25 mm, followed by curing. Using a Teflon tape spacer (AGF-100FR, Chukoh Chemical Industries, Ltd.), the thickness of the adhesive layer was maintained at 0.18 mm. The lap shear strength was defined as the maximum stress required to destroy the bonded specimen. Stress was calculated by dividing the applied force by the adhesion area (12.5 mm × 25 mm) and was evaluated using a UTM (5982, Instron). The lap shear strength test was repeated five times, and all experiments were conducted at room temperature (23 °C).

3. Results and discussion

3.1. Design and synthesis

To overcome the inherent limitations in epoxy toughening, particularly in achieving an optimal balance between flexibility, toughness, and thermal properties, we explored a novel approach using urethane linkages to create an aliphatic diol-based toughening system. As shown in Fig. 1(a), unlike conventional toughening methods that often result in undesirable trade-offs between impact resistance and mechanical properties such as stiffness, our approach leverages phase separation with tunable domain sizes along with urethane modification to enhance both the mechanical and thermal stability of the epoxy matrix. We synthesized aliphatic diols by polymerizing propylene carbonate with Jeffamine-230 and Jeffamine-400, which vary in chain length, to create urethane linkages. These urethane-modified aliphatic diols were subsequently introduced as additives into the epoxy matrix. Specifically, A-D230 and A-D400 were used to form phase separation domains within the epoxy matrix, which retained its inherent rigid properties. By varying the diol content from 10 % to 50 %, we induced a controlled phase separation, with the domain sizes gradually evolving into a bicontinuous phase separation structure as the content increased.

In this phase-separated structure, the domains formed by the urethane-based aliphatic diols act as energy absorption centers. Upon impact or under dynamic loading, these domains effectively absorb and redistribute the stress across multiple domains, thereby delaying failure. Furthermore, this phase separation design is expected to enhance the fatigue durability under sustained small stresses, as it prevents crack initiation and propagation by distributing stresses more uniformly throughout the material. The nanoscale domain size and their distribution are critical in enhancing both impact resistance and elongation without compromising the structural integrity of the epoxy matrix [32,33].

However, recognizing that phase separation may introduce trade-offs, particularly in thermal properties and adhesion performance, we addressed these potential limitations by synthesizing urethane-modified epoxy [24]. This was achieved by reacting the aliphatic diol (previously used as an additive) with epichlorohydrin under thermal conditions in the presence of sodium hydroxide (NaOH) and a catalytic amount of tetrabutylammonium bromide (TBAB). The resulting urethane-modified epoxy possesses terminal epoxide groups, allowing it to react with amines and integrate homogeneously into the epoxy matrix.

Unlike the bicontinuous phase separation observed with the aliphatic diol additives, the urethane-modified epoxy forms a uniform, single-phase network. This structure ensures consistent mechanical properties throughout the material, leading to higher cross-link density, improved thermal stability, and enhanced shear strength. The urethane linkages introduced during synthesis increase toughness while maintaining high thermal and mechanical stability, making the material particularly suitable for applications requiring both impact resistance and high thermal performance.

3.2. Morphology analysis

To confirm the formation of separate phases and examine the size and distribution of the domains, four analytical methods were employed. First, small-angle X-ray scattering (SAXS) was used to assess the scattering peaks of the DGEBA, A-D230 50 %, A-D400 50 %, R-U230 50 %, and R-U400 50 % samples, as shown in Fig. 1(b). Among these, distinct scattering peaks were observed only in the A-D400 50 % sample, while A-D230 50 % displayed the same scattering profile as the reactants and DGEBA, suggesting the absence of significant phase separation. Fig. 1(c) further illustrates the change in scattering intensity with increasing A-D400 content. At 10 % content, no scattering was observed, similar to the case of homogeneous samples, but as the concentration increased, the scattering intensity rose, indicating growth of the domain size and formation of larger bicontinuous domains [34,35].

Next, we examined the transparency of the DGEBA, A-D230 50 %, A-D400 50 %, R-U230 50 %, and R-U400 50 % samples. As depicted in Fig. 1(d), all samples, including those with significant phase separation (A-D400 50 %), remained transparent, with no reduction in light transmittance. This suggests that the phase-separated domain sizes are in the nanometer range, smaller than the wavelength of visible light, and

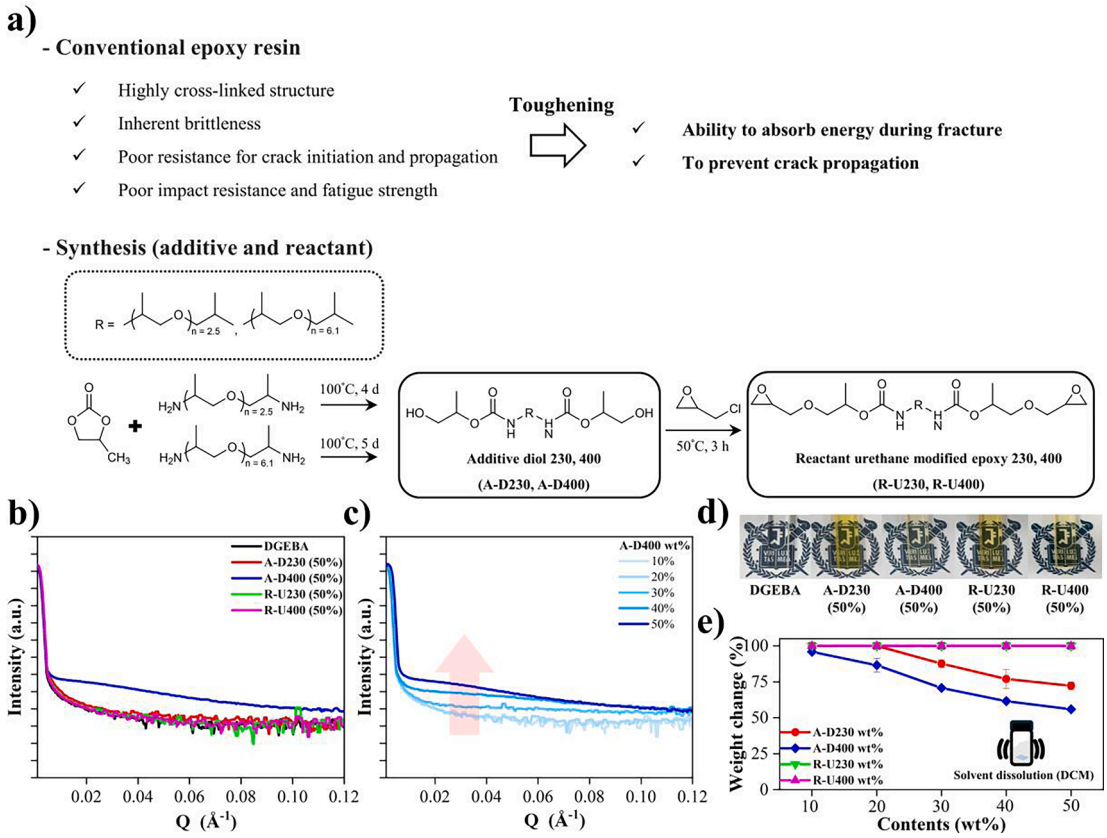

Fig. 1. a) synthesis of additive and reactant; b), c) saxs scattering patterns; d) transparency evaluation; e) solvent dissolution and corresponding weight loss measurements.

thus do not affect optical transparency.

To further investigate the size and distribution of the phase-separated domains, solvent dissolution using DCM was performed. The weight changes of the DGEBA, A-D230, A-D400, R-U230, and R-U400 samples before and after dissolution are shown in Fig. 2. This method provides insights into the amount and size of the phase-separated domains. DGEBA, R-U230, and R-U400 showed no dissolution, indicating resistance to solvent penetration due to high cross-link density. In the case of A-D230, no dissolution was observed at 10 % and 20 % concentrations, suggesting that small, isolated island domains were formed, which could not be penetrated by the solvent [36,37]. At higher concentrations (30–50 %), A-D230 showed weight losses of 100 %, 87.7 %, 77 %, and 72.2 %, indicating the formation of bicontinuous structures as well as isolated domains. The 50 % sample exhibited 27.8 % bicontinuous structure and 22.2 % isolated domains.

For A-D400, the results were different. The weight losses were 95.8 %, 86.6 %, 70.7 %, 61.6 %, and 56 %, suggesting that as the content of A-D400 increased, the bicontinuous structure became more dominant. The A-D400 50 % sample exhibited 44 % bicontinuous structure and only 6 % isolated phase, indicating a greater degree of interconnected domains compared to A-D230.

Finally, scanning electron microscopy (SEM) was used to visually analyze the phase-separated microstructure after solvent dissolution. SEM analysis was conducted on the samples that exhibited weight changes, allowing for the identification of the size and distribution of the domains [38]. For A-D230, the 30 %, 40 %, and 50 % samples were examined, in which only the bicontinuous structure was dissolved, leaving behind isolated domains. Consistent with the SAXS data, the bicontinuous domains in A-D230 were extremely small and difficult to observe in SEM. In contrast, the SEM images of A-D400 revealed clear bicontinuous domains that increased in size as the concentration increased. At 40 % concentration, domains ranging from approximately 100 nm to 600 nm were observed. At 50 % concentration, the bicontinuous regions became more prominent, with the largest domains reaching over 900 nm, confirming that increasing the content of A-D400 leads to larger bicontinuous structures.

3.3. Mechanical performance (Tensile strength)

Tensile testing of DGEBA, A-D230, A-D400, R-U230, and R-U400 was conducted. As shown in Fig. 3(a), an improvement in the ductility of A-D230 was observed up to 40 % concentration, but the material overall exhibited a brittle tendency. This indicates that the isolated domains were insufficient to disperse stress effectively before significant deformation occurred, leading to early failure. At 50 % concentration of A-D230, the elongation at break increased sharply to 10.5 %, suggesting that smaller domain sizes in phase-separated structures promote more efficient stress distribution. As shown in Fig. 3(b), A-D400 exhibited larger domain sizes compared to A-D230 and showed ductility improvements for concentrations over 30 %. However, at 50 % concentration of A-D400, the elongation at break was 5.1 %, which is significantly lower than that of A-D230 at 50 %. This result implies that larger domain sizes reduce the pathways for stress distribution within the material, leading to less efficient stress dispersion. The presence of smaller domains creates more pathways for uniform stress distribution within the material, preventing stress concentration and contributing to more effective stress dissipation [39–41]. Conversely, larger domain sizes, as in A-D400, tend to localize stress and absorb energy in specific regions but are less effective at distributing and dissipating stress throughout the material. Thus, smaller domain sizes improve the material's deformation and fracture resistance, allowing for better energy absorption and enhanced toughness.

To further investigate these trends, tensile tests were conducted on A-D230 50 % and A-D400 50 % at varying strain rates (1, 5, 10, 20, 40,

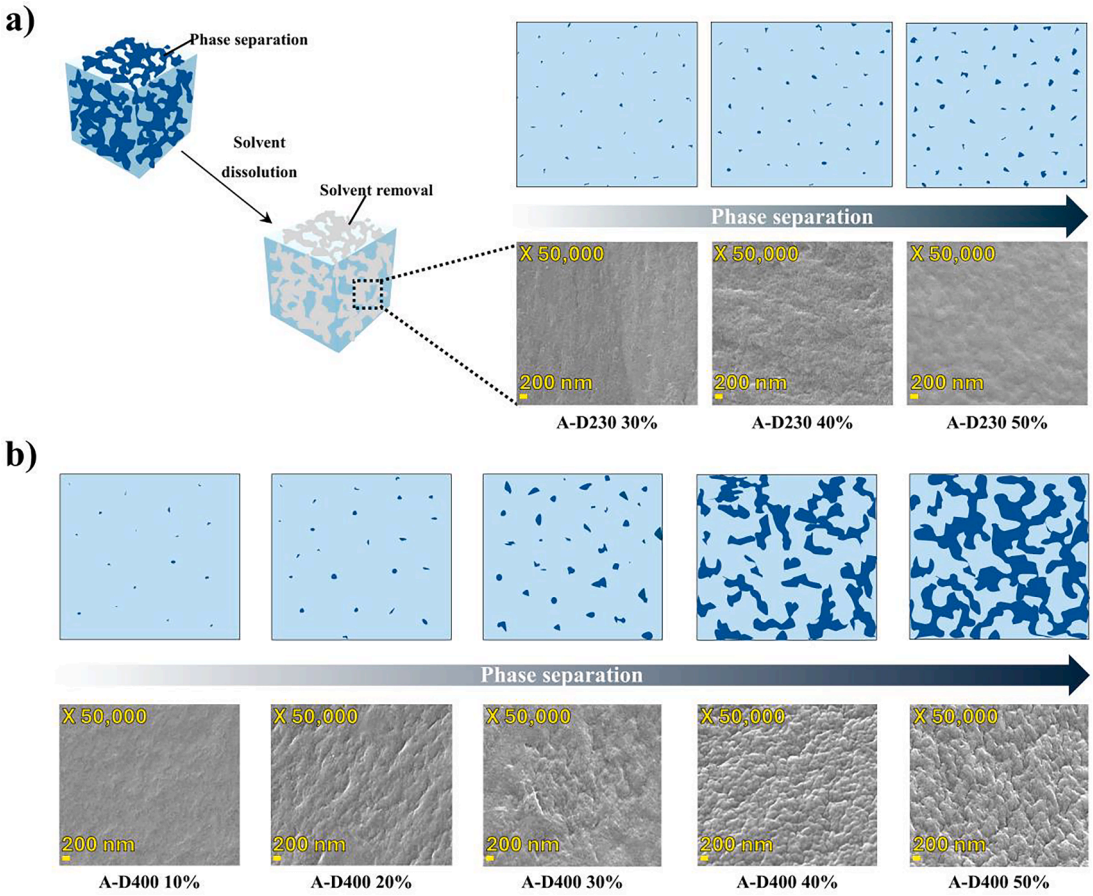

Fig. 2. Top: schematic of phase separation, bottom: SEM surface observations after solvent dissolution a) A-D230 wt%, b) A-D400 wt%.

and 80 mm/min). As shown in Fig. 3(c), at lower strain rates, smaller domains were more effective in dispersing impact energy and dissipating applied energy. At a strain rate of 1 mm/min, the stress level increased, and the elongation at break reached 12 %, indicating that smaller domains had sufficient time to distribute the stress throughout the material, preventing stress concentration. However, as the strain rate increased, the smaller domains in A-D230 had less time to absorb and disperse energy, leading to stress concentration and material failure. At strain rates of 40 mm/min and above, the material was unable to effectively distribute stress, resulting in significantly lower elongation at break. At 80 mm/min, the elongation dropped to 4 %. These findings suggest that A-D230, with its smaller domains, is more effective in environments with fatigue stress or small, accumulated stresses over time. The strain-rate-dependent tensile test results for A-D400 50 % are shown in Fig. 3(d). Unlike A-D230, A-D400 exhibited relatively low stress at low strain rates, indicating a reduced capacity for effective energy dispersion and dissipation. Interestingly, as the strain rate increased, A-D400 displayed higher elongation at break. This can be attributed to its larger domain sizes, which, at higher strain rates, could absorb the greater instantaneous stress. Thus, as the strain rate increased, A-D400 exhibited higher elongation, indicating that the larger domains are more suited to absorbing high impact energy. In contrast, A-D230, with its smaller domains, was less effective at absorbing high impact energy, showing lower elongation at higher strain rates. These results highlight how the domain size in each material significantly influences the material's mechanical performance depending on the strain rate.

Compared to phase separation, uniform dispersion is reduced, concentrating stress in specific areas and leading to localized weakening. Consequently, in terms of elongation properties, additive materials exhibit higher elongation rates compared to reactant materials due to these underlying mechanisms.

The tensile test results for reactants 230 and 400 show lower elongation compared to the additives, as observed in Fig. 4. Fig. 4(a) shows that the short urethane chains in R-U230 bond with the epoxy matrix, forming a dense and highly crosslinked network. This results in high tensile strength, even at 50 % content, due to the material's effective resistance to deformation. However, the flexibility of the short chains is limited, and the high crosslink density restricts chain mobility, leading to earlier failure under tensile stress, as the material cannot stretch sufficiently before breaking.

As shown in Fig. 4b, R-U400 exhibits lower tensile strength than R-U230, but at 50 % content, it achieves an elongation of 3 %. The longer urethane chains provide greater flexibility and mobility, forming a less densely crosslinked network. This allows the material to absorb more energy before failure, indicating improved ductility compared to R-U230.

3.4. *Mechanical performance (Impact strength)*

The Izod impact test results are expected to follow a similar trend to the tensile strength tests performed at high strain rates. This test measures a material's resistance to high-impact forces, reflecting its toughness and energy absorption capacity. The DGEBA sample, known for its inherent brittleness, exhibited the lowest impact strength, as anticipated. Fig. 5(a) presents the impact strength values for A-D230 (20.7, 22.6, 24.3, 29, 35.3 J/m). Similar to the results of the high-strain-rate tensile tests, the impact strength increased with increasing additive content. However, A-D230 still showed relatively low impact strength compared to other formulations, aside from DGEBA. This can be attributed to the small phase-separated domains in A-D230. While these

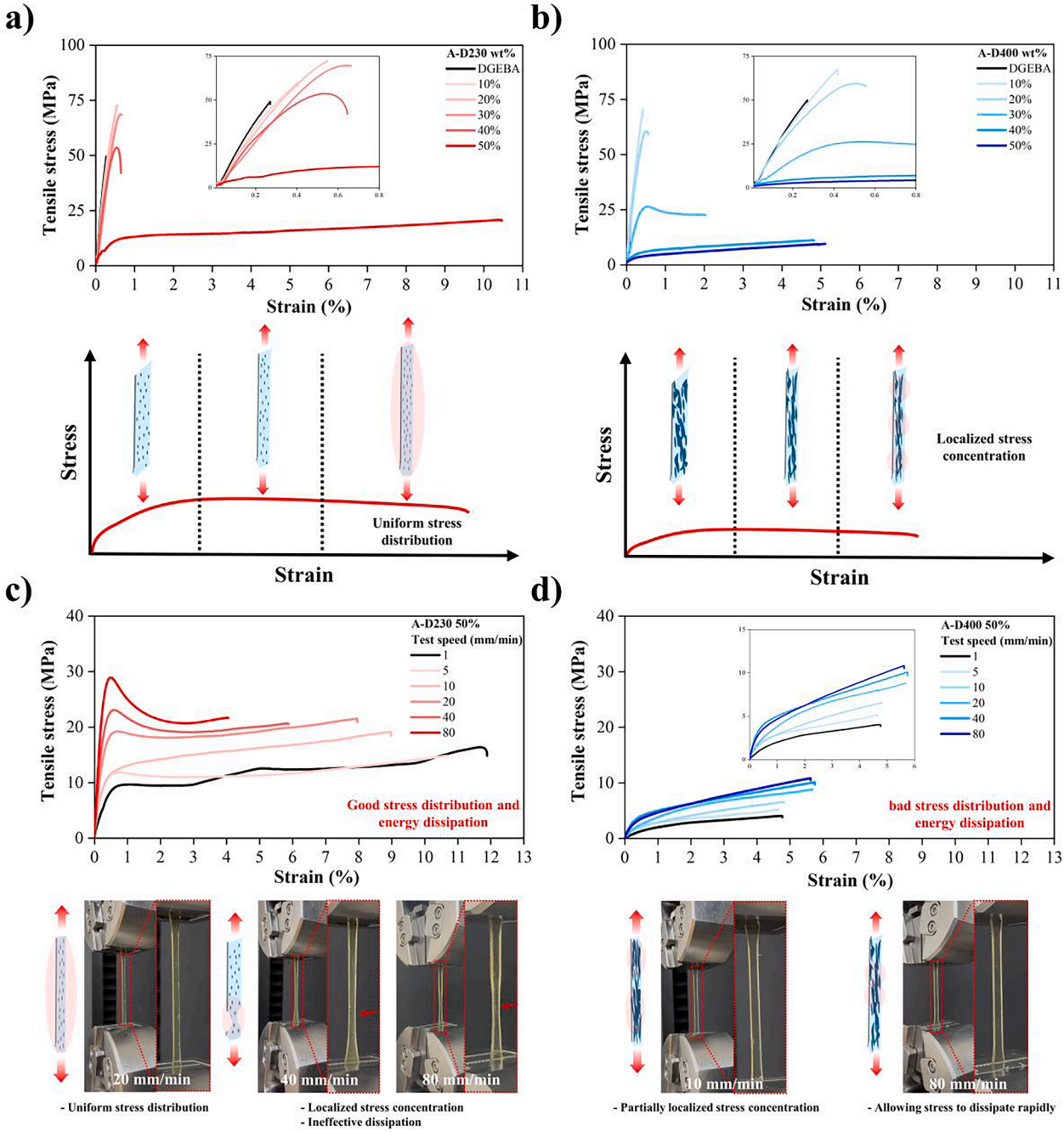

Fig. 3. Tensile strength s-s curves: (a) A-D230 wt%, (b) A-D400 wt%, tensile strength test speeds (1, 5, 10, 20, 40, 80 mm/min), (c) A-D230 50 %, (d) A-D400 50 %.

small domains can effectively distribute low-level stresses, they are too small to absorb high-impact energy sufficiently, leading to localized stress concentrations. As a result, these small domains accelerate crack initiation and propagation, further reducing the material's impact resistance [42]. On the other hand, A-D400 exhibited significantly higher impact strength as its content increased (24, 31.4, 37.3, 69.7, 72 J/m). The larger phase-separated domains in A-D400 can effectively absorb and dissipate impact energy, making the material more resistant to high-impact forces. The fracture surface analysis also confirmed that these larger, interconnected domains prevent localized stress concentrations and delay crack propagation by promoting crack pinning and stress dispersion across multiple pathways [43–45].

In R-U230 (32.1, 37.7, 37.2, 44.2, 44.6 J/m), a slight increase in impact strength was observed. Fig. 5(b) shows that R-U400 (35.5, 36.8, 45.8, 49.1, 56.1 J/m) also demonstrated high impact strength. The urethane-modified epoxy in these samples provides a uniform structure that allows the material to evenly absorb impact energy across the matrix. Although R-U230 shows slightly lower impact strength than R-U400 due to its shorter urethane linkages, it still performs well under impact, as there are no localized stress concentrations in phase-separated systems. Instead, the material absorbs energy uniformly, resulting in improved impact resistance. Fracture surface analysis of R-U230 and R-U400 revealed distinct fracture patterns compared to the phase-separated samples. The flexible urethane network in these systems uniformly absorbs the impact across the matrix, leading to rougher fracture surfaces under high-impact conditions, as the entire material structure engages in absorbing and distributing the stress.

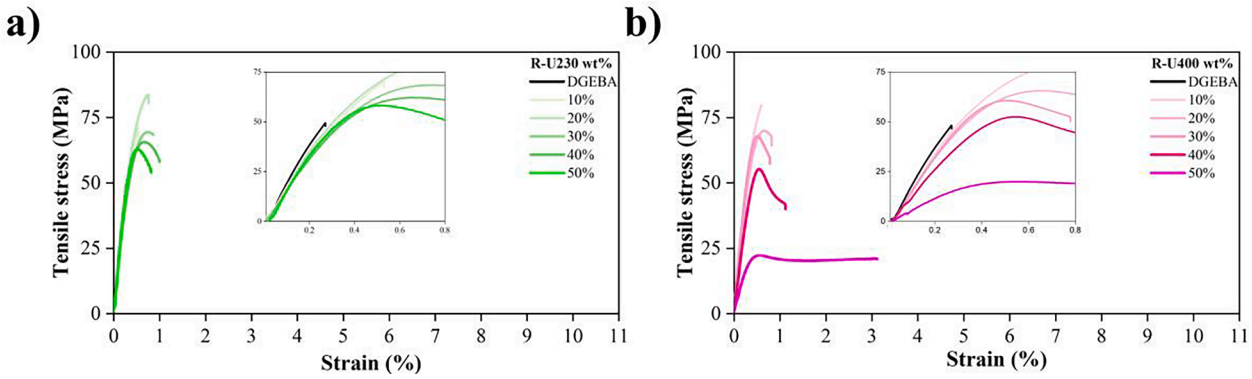

Fig. 4. Tensile strength s-s curves: (a) R-U230 wt%, (b) R-U400 wt%.

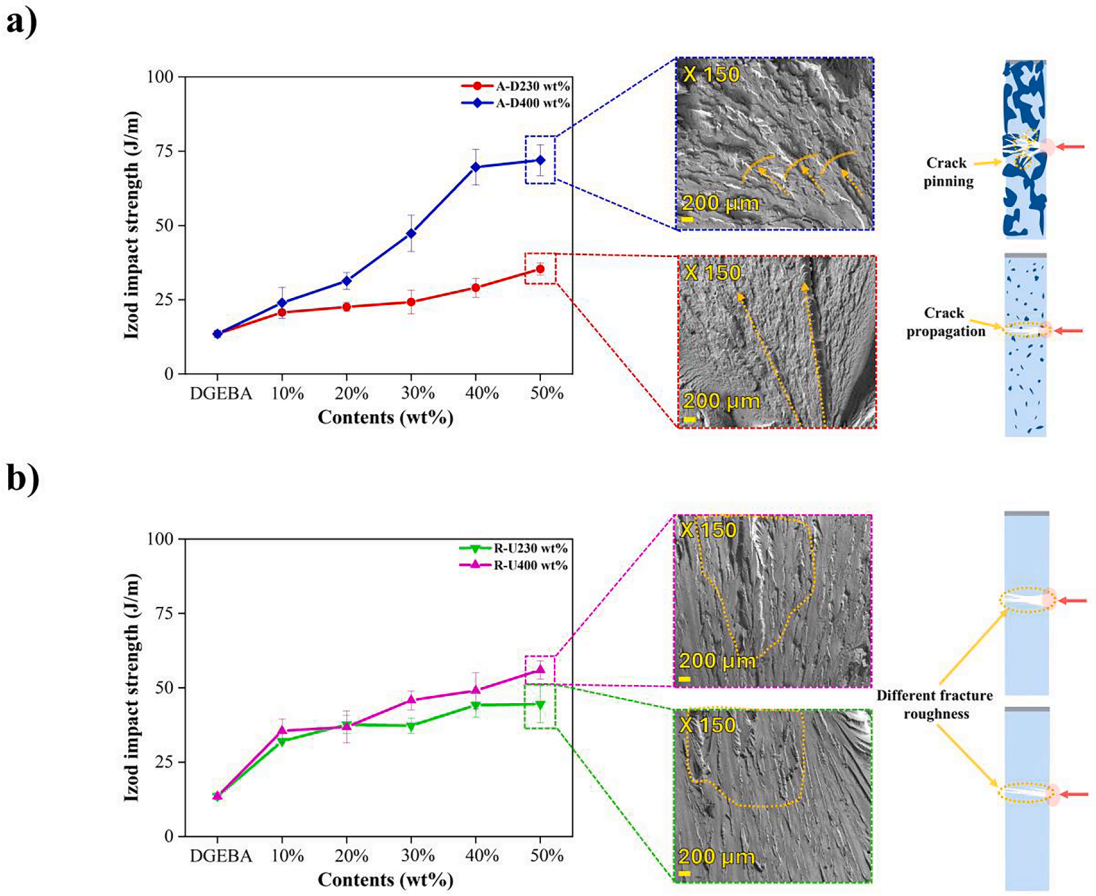

Fig. 5. Izod impact strength (a) A-D230 wt%, A-D400 wt%, (b) R-U230 wt%, R-U400 wt%.

3.5. Dynamic mechanical thermal analysis

Dynamic Mechanical Analysis (DMA) was conducted to evaluate the thermal stability of the materials. After the glass transition temperature (Tg), the material transitions into a rubber-like, flexible state, making Tg a crucial indicator of a material's thermal stability and resistance to thermal deformation. As illustrated in Figs. S1 and S2, for A-D230 and A-D400, the storage modulus decreases significantly with an increase in additive content. In contrast, R-U230 and R-U400 maintained more stable storage modulus values compared to the additive-based samples. This behavior is attributed to the presence of phase-separated domains, which introduce soft and flexible regions within the polymer matrix, reducing the overall cross-link density that typically holds the polymer chains together. Consequently, as seen in Fig. 6(a), (b), (c), and (d), the cross-linking density and Tg are significantly affected [46,47].

As the proportion of bulk epoxy decreases during the phase separation process, the presence of phase-separated domains increases with the addition of A-D230 and A-D400. This change induces the formation of phase-separated domains within the epoxy network. When the bulk epoxy proportion decreases by 10 %, the cross-linking between polymer chains is reduced, leading to a decrease in mechanical strength and stiffness. This reduction in cross-linking density results in a more relaxed network, which in turn increases the material's flexibility. With an increasing A-D230 content, the cross-linking density decreases from 27,217 mol/m3 to 8,414 mol/m3, which reduces stiffness but increases elongation. Particularly, longer chains result in a greater reduction in cross-linking density and stiffness, with A-D400 showing a larger reduction compared to A-D230, decreasing from 27,217 mol/m3 to

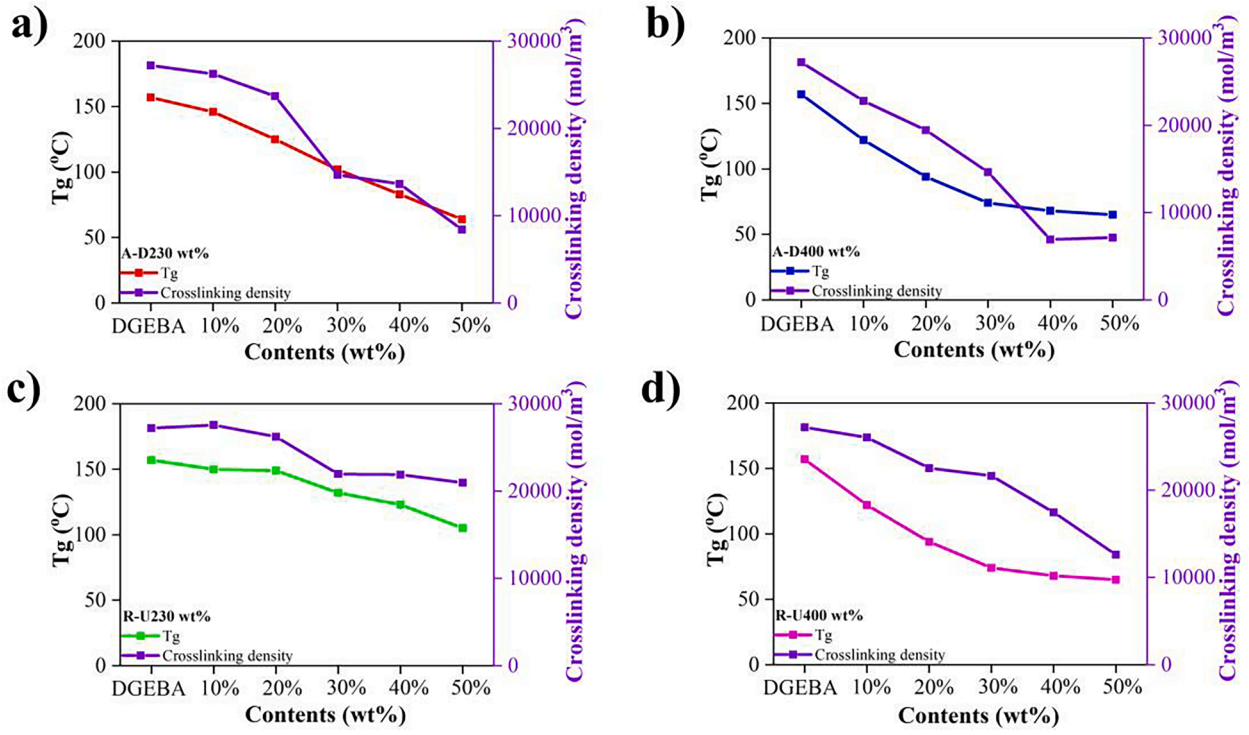

Fig. 6. Tg and crosslinking density a) A-D230 wt%, (b) A-D400 wt%, (c) R-U230 wt%, (d) R-U300 wt%.

7,143 mol/m3. In addition, thermal stability, which is closely related to cross-linking density, is also significantly affected as the bulk epoxy proportion decreases. When cross-linking density decreases due to phase separation, there is more space for polymer chains to move freely, leading to a decrease in the glass transition temperature (Tg), indicating a reduction in thermal stability.

On the other hand, R-U230 maintains a high cross-linking density of 27,563 mol/m^3, even at an additive concentration of 50 % where the

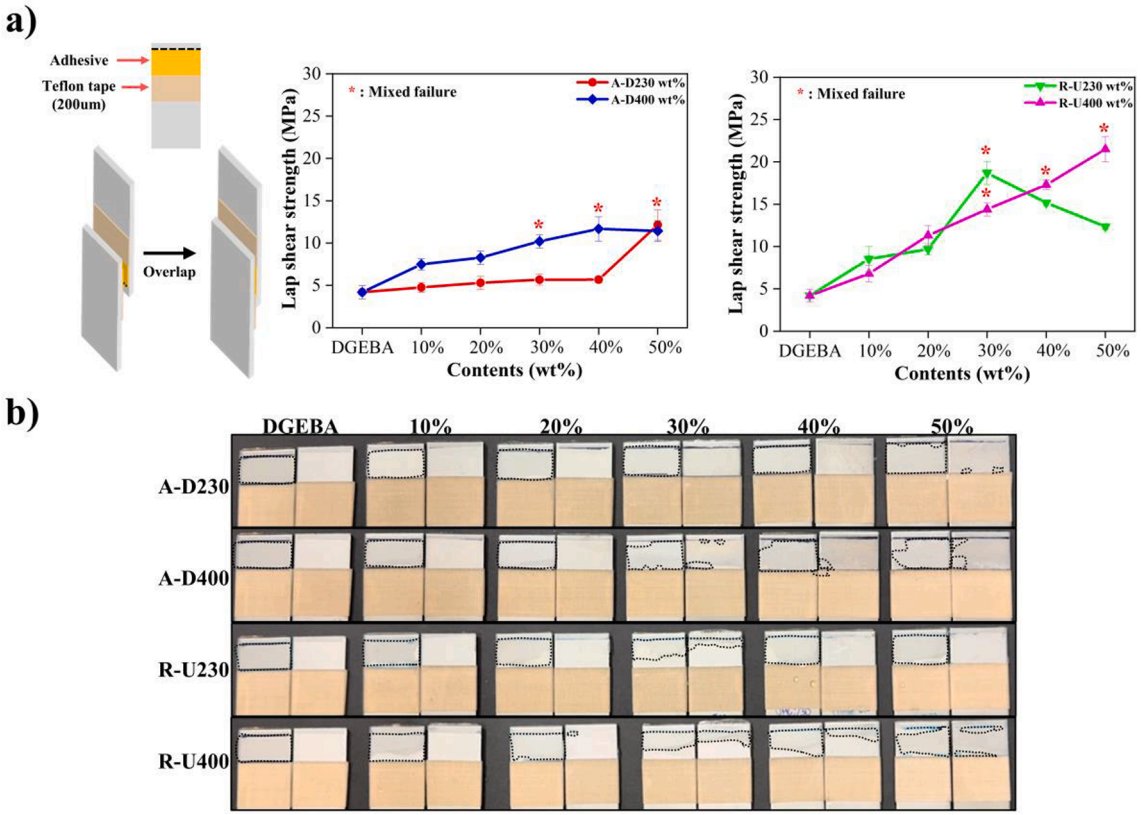

Fig. 7. Lap shear strength a) (left) A-D230 wt%, A-D400 wt% (right) R-U230 wt%, R-U400 wt%, (b)) adhesive failure shape.

value remains at 20,954 mol/m^3. Similarly, R-U400 decreases from 26,051 mol/m^3 to 12,620 mol/m^3 at 50 %, but still retains relatively high cross-linking density. This high cross-linking density suggests that the urethane linkages form a more uniform and stable network structure, contributing to greater thermal stability. Thus, R-U230 and R-U400 demonstrate superior thermal stability and are expected to provide more reliable performance in high-temperature environments.

3.6. Lap shear strength and observation of adhesive failure

The lap shear strength results in Fig. 7(a) show the performance differences between the base DGEBA epoxy, the phase-separated systems (A-D230 and A-D400), and the urethane-modified epoxies (R-U230 and R-U400). The shear strength of A-D230 and A-D400 gradually improves with increasing content. For A-D230, the shear strength increased from 4.8 MPa to 12.1 MPa, whereas for A-D400, it increased from 7.5 MPa to 11.7 MPa before slightly decreasing to 11.4 MPa. As shown in the adhesive failure morphology in Fig. 7(b), A-D230 and A-D400 predominantly exhibit interfacial failure, along with small areas of mixed failure mode.

In contrast, R-U230 and R-U400 exhibited significantly higher shear strengths compared to the phase-separated systems. At 10 % concentration, the shear strength of R-U230 was 8.5 MPa, which increased and peaked at 18.7 MPa at 30 % content before decreasing to 12.4 MPa at 50 % concentration. The decrease in shear strength at higher content levels is attributed to excessive flexibility, which reduces the structural integrity of the material. Excessive flexibility may lead to localized stress concentration, causing the material to fail more easily. The shear strength of R-U400, on the other hand, steadily increased from 6.79 MPa at 10 % content to 21.5 MPa at 50 % content. The urethane modification in the epoxy facilitates strong chemical bonding between the epoxy matrix and the substrate, promoting a more uniform distribution of shear stress across the material, thereby enhancing shear strength. As shown in Fig. 7(b), the mixed failure mode indicates that both the adhesive and substrate exhibit failure evenly at the interface.

The phase-separated structures, however, form only covalent bonds in the epoxy matrix, excluding the phase-separated regions. Although these domains can help distribute stress through physical interactions or intermolecular forces, they do not establish strong chemical bonds with the substrate, which can result in a reduction in overall shear strength. Based on these observations, due to their uniform network structure and stronger adhesive bonding, R-U230 and R-U400 are more suitable for applications requiring high shear strength.

This study developed aliphatic diol-based materials to overcome the limitations of conventional rubber-based toughening agents and to enhance mechanical properties. To evaluate their performance, a direct comparison of mechanical properties, including shear strength, impact strength, and elongation, was conducted between the commercial CSR pre-dispersed DGEBA resin (35 wt%) (KDAD-7101, Kukdo Chemical) and phase-separated materials (A-D230, A-D400, 50 wt%), as illustrated in Fig. 8. The experimental results revealed that KDAD exhibited the highest lap shear strength, reaching 17.8 MPa. However, its elongation was exceptionally low at 0.65 %, indicating minimal improvement compared to conventional epoxy systems. This low elongation is likely to result in reduced fatigue resistance under cyclic deformation. Furthermore, KDAD demonstrated lower impact strength compared to A-D400, which forms larger phase-separated domains.

In contrast, the aliphatic diol-based materials demonstrated a significant advantage in both impact strength and elongation. The ability to achieve higher values in both properties highlights the potential of these materials to address the inherent trade-off often observed between toughness and ductility in conventional epoxy toughening systems. The enhanced performance is attributed to the nano- and micro-scale phase-separated domains, which facilitate effective stress absorption and redistribution, leading to improved mechanical behavior under dynamic and static loading conditions.

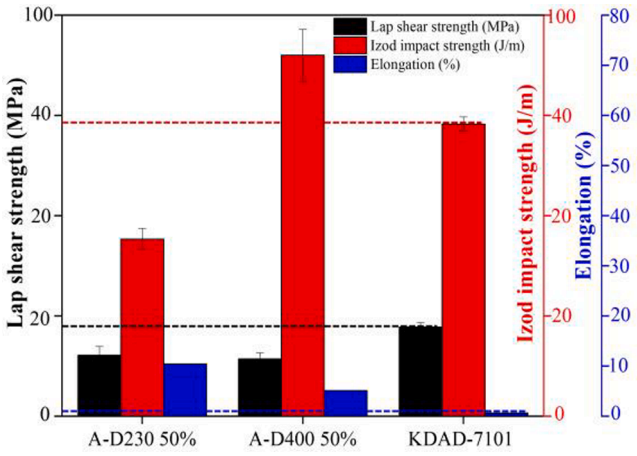

Fig. 8. Comparison of mechanical properties between commercial CSR pre-dispersed DGEBA resin.

4. Conclusion

This study has successfully demonstrated the potential of phase separation and urethane modification strategies in enhancing the toughness, adhesion, and thermal stability of epoxy resins, particularly for demanding applications such as automotive adhesives. The incorporation of aliphatic diols with urethane linkages formed nano-sized domains within the epoxy matrix, promoting uniform stress distribution and efficient energy absorption. This resulted in improved impact resistance and elongation, especially in the A-D230 and A-D400 formulations, with the latter exhibiting superior performance under high-impact conditions due to its larger domain structures.

Additionally, the urethane-modified epoxy systems (R-U230 and R-U400) displayed enhanced thermal stability and shear strength, which are attributed to their homogeneous network structures. The increased cross-linking density in these systems contributed to superior mechanical integrity, making them suitable for high-performance applications that demand both mechanical strength and thermal resilience.

By leveraging phase-separated structures in conjunction with urethane modifications, this research addresses key limitations in traditional epoxy toughening strategies. The findings present a promising pathway for developing customized epoxy systems that can meet the specific requirements of various industrial applications, particularly where durability, flexibility, and long-term reliability are critical. These results provide a solid foundation for future innovations in epoxy formulations, advancing their use in high-performance adhesive applications.

CRediT authorship contribution statement

Kyeng-Bo Sim: Writing – original draft, Methodology, Conceptualization. **Jong-Ho Back:** Visualization, Conceptualization. **Gi-Yeon Han:** Investigation, Data curation. **Hyun-Joong Kim:** Supervision.

Declaration of competing interest

The authors declare that they have no known competing financial interests or personal relationships that could have appeared to influence the work reported in this paper.

Acknowledgments

This work was supported by the Technology Innovation Program (grant number 20010768, Development of Fast Curing Structural Adhesive with High Performance for Dissimilar Materials in High Speed Processes) funded by the Ministry of Trade, Industry & Energy (MOTIE,

Korea).

Appendix A. Supplementary material

Supplementary data to this article can be found online at https://doi.org/10.1016/j.compositesa.2024.108652.

Data availability

Data will be made available on request.

References

[1] Jin FL, Li X, Park SJ. Synthesis and application of epoxy resins: a review. J Ind Eng Chem 2015;29:1–11. https://doi.org/10.1016/j.jiec.2015.03.026.

[2] Vidil T, Tournilhac F, Musso S, Robisson A, Leibler L. Control of reactions and network structures of epoxy thermosets. Prog Polym Sci 2016;62:126–79. https://doi.org/10.1016/j.progpolymsci.2016.06.003.

[3] Mi X, Liang N, Xu H, Wu J, Jiang Y, Nie B, et al. Toughness and its mechanisms in epoxy resins. Prog Mater Sci 2022;130. https://doi.org/10.1016/j.pmatsci.2022.100977.

[4] Czaderski C, Martinelli E, Michels J, Motavalli M. Effect of curing conditions on strength development in an epoxy resin for structural strengthening. Compos B Eng 2012;43:398–410. https://doi.org/10.1016/j.compositesb.2011.07.006.

[5] Qiu Y, Qian L, Chen Y, Hao J. Improving the fracture toughness and flame retardant properties of epoxy thermosets by phosphaphenanthrene/siloxane cluster-like molecules with multiple reactive groups. Compos B Eng 2019;178. https://doi.org/10.1016/j.compositesb.2019.107481.

[6] Seo J, Yui N, Seo JH. Development of a supramolecular accelerator simultaneously to increase the cross-linking density and ductility of an epoxy resin. Chem Eng J 2019;356:303–11. https://doi.org/10.1016/j.cej.2018.09.020.

[7] Kim BC, Park SW, Lee DG. Fracture toughness of the nano-particle reinforced epoxy composite. Compos Struct 2008;86:69–77. https://doi.org/10.1016/j.compstruct.2008.03.005.

[8] Domun N, Hadavinia H, Zhang T, Sainsbury T, Liaghat GH, Vahid S. Improving the fracture toughness and the strength of epoxy using nanomaterials-a review of the current status. Nanoscale 2015;7:10294–329. https://doi.org/10.1039/c5nr01354b.

[9] Jayan JS, Saritha A, Joseph K. Innovative materials of this era for toughening the epoxy matrix: a review. Polym Compos 2018;39:E1959–86. https://doi.org/10.1002/pc.24789.

[10] Roy S, Petrova RS, Mitra S. Effect of carbon nanotube (CNT) functionalization in epoxy-CNT composites. Nanotechnol Rev 2018;7:475–85. https://doi.org/10.1515/ntrev-2018-0068.

[11] Kumar S, Krishnan S, Samal SK, Mohanty S, Nayak SK. Toughening of petroleum based (DGEBA) epoxy resins with various renewable resources based flexible chains for high performance applications: a review. Ind Eng Chem Res 2018;57:2711–26. https://doi.org/10.1021/acs.iecr.7b04495.

[12] Liu Y. Polymerization-induced phase separation and resulting thermomechanical properties of thermosetting/reactive nonlinear polymer blends: a review. J Appl Polym Sci 2013;127:3279–92. https://doi.org/10.1002/app.38721.

[13] Mansour G, Tsongas K, Tzetzis D. Investigation of the dynamic mechanical properties of epoxy resins modified with elastomers. Compos B Eng 2016;94:152–9. https://doi.org/10.1016/j.compositesb.2016.03.024.

[14] Zhou L, Fu Y, Yin T, Luo Z. Synergetic effect of epoxy resin and carboxylated nitrile rubber on tribological and mechanical properties of soft paper-based friction materials. Tribol Int 2019;129:314–22. https://doi.org/10.1016/j.triboint.2018.08.020.

[15] Saleh ABB, Ishak ZAM, Hashim AS, Kamil WA, Ishiaku US. Synthesis and characterization of liquid natural rubber as impact modifier for epoxy resin. Phys Procedia, vol. 55, Elsevier B.V.; 2014, p. 129–37. DOI: 10.1016/j.phpro.2014.07.019.

[16] Quan D, Ivankovic A. Effect of core-shell rubber (CSR) nano-particles on mechanical properties and fracture toughness of an epoxy polymer. Polymer (Guildf) 2015;66:16–28. https://doi.org/10.1016/j.polymer.2015.04.002.

[17] Baek D, Sim KB, Kim HJ. Mechanical characterization of core-shell rubber/epoxy polymers for automotive structural adhesives as a function of operating temperature. Polymers (Basel) 2021;13:1–18. https://doi.org/10.3390/polym13050734.

[18] Hou W, Gao Y, Wang J, Blackwood DJ, Teo S. Recent advances and future perspectives for graphene oxide reinforced epoxy resins. Mater Today Commun 2020;23. https://doi.org/10.1016/j.mtcomm.2019.100883.

[19] Dong M, Zhang H, Tzounis L, Santagiuliana G, Bilotti E, Papageorgiou DG. Multifunctional epoxy nanocomposites reinforced by two-dimensional materials: a review. Carbon N Y 2021;185:57–81. https://doi.org/10.1016/j.carbon.2021.09.009.

[20] Mousavi SR, Estaji S, Paydayesh A, Arjmand M, Jafari SH, Nouranian S, et al. A review of recent progress in improving the fracture toughness of epoxy-based composites using carbonaceous nanofillers. Polym Compos 2022;43:1871–86. https://doi.org/10.1002/pc.26518.

[21] Vijayan PP, Puglia D, Al-Maadeed MASA, Kenny JM, Thomas S. Elastomer/thermoplastic modified epoxy nanocomposites: the hybrid effect of 'micro' and 'nano' scale. Mater Sci Eng R Rep 2017;116:1–29. https://doi.org/10.1016/j.mser.2017.03.001.

[22] Lu S, Ban J, Yu C, Deng W. Properties of Epoxy Resins Modified with Liquid Crystalline Polyurethane. n.d.

[23] Zhang X, Gu A, Liang G, Zhuo D, Yuan L. Liquid crystalline epoxy resin modified cyanate ester for high performance electronic packaging. J Polym Res 2011;18:1441–50. https://doi.org/10.1007/s10965-010-9549-3.

[24] Leguizamon SC, Powers J, Ahn J, Dickens S, Lee S, Jones BH. Polymerization-induced phase separation in rubber-toughened amine-cured epoxy resins: tuning morphology from the nano- to macro-scale. Macromolecules 2021;54:7796–807. https://doi.org/10.1021/acs.macromol.1c01208.

[25] Zheng N, Sun W, Liu HY, Huang Y, Gao J, Mai YW. Effects of carboxylated carbon nanotubes on the phase separation behaviour and fracture-mechanical properties of an epoxy/polysulfone blend. Compos Sci Technol 2018;159:180–8. https://doi.org/10.1016/j.compscitech.2018.02.039.

[26] Li J, Zhu W, Zhang S, Gao Q, Li J, Zhang W. Amine-terminated hyperbranched polyamide covalent functionalized graphene oxide-reinforced epoxy nanocomposites with enhanced toughness and mechanical properties. Polym Test 2019;76:232–44. https://doi.org/10.1016/j.polymertesting.2019.03.017.

[27] He R, Zhan X, Zhang Q, Chen F. Toughening of an epoxy thermoset with poly [styrene-Alt-(maleic acid)]-block-polystyrene-block-poly(n-butyl acrylate) reactive core-shell particles. RSC Adv 2016;6:35621–7. https://doi.org/10.1039/c6ra05048d.

[28] Stevens MJ. Simulation of polymerization induced phase separation in model thermosets. J Chem Phys 2021;155. https://doi.org/10.1063/5.0061654.

[29] Kawagoe Y, Kikugawa G, Shirasu K, Kinugawa Y, Okabe T. Dissipative particle dynamics simulation for reaction-induced phase separation of thermoset/thermoplastic blends. J Phys Chem B 2024;128:2018–27. https://doi.org/10.1021/acs.jpcb.3c07756.

[30] Brooker RD, Kinloch AJ, Taylor AC. The morphology and fracture properties of thermoplastic-toughened epoxy polymers. J Adhes 2010;86:726–41. https://doi.org/10.1080/00218464.2010.482415.

[31] Kishi H, Tanaka S, Nakashima Y, Saruwatari T. Self-assembled three-dimensional structure of epoxy/polyethersulphone/silver adhesives with electrical conductivity. Polymer (Guildf) 2016;82:93–9. https://doi.org/10.1016/j.polymer.2015.11.043.

[32] Wang M, Zhang P, Shamsi M, Thelen JL, Qian W, Truong VK, et al. Tough and stretchable ionogels by in situ phase separation. Nat Mater 2022;21:359–65. https://doi.org/10.1038/s41563-022-01195-4.

[33] Okada M, Fujimoto K, Nose T. Phase Separation Induced by Polymerization of 2-Chlorostyrene in a Polystyrene/Dibutyl Phthalate Mixture. vol. 28. 1995.

[34] Chopade SA, So S, Hillmyer MA, Lodge TP. Anhydrous proton conducting polymer electrolyte membranes via polymerization-induced microphase separation. ACS Appl Mater Interfaces 2016;8:6200–10. https://doi.org/10.1021/acsami.5b12366.

[35] Chopade SA, Au JG, Li Z, Schmidt PW, Hillmyer MA, Lodge TP. Robust polymer electrolyte membranes with high ambient-temperature lithium-ion conductivity via polymerization-induced microphase separation. ACS Appl Mater Interfaces 2017;9:14561–5. https://doi.org/10.1021/acsami.7b02514.

[36] Billet R, Zeng B, Lockhart J, Gattrell M, Zhao H, Zhang X. Dissolution dynamics of a binary switchable hydrophilicity solvent-polymer drop into an acidic aqueous phase. Soft Matter 2022. https://doi.org/10.1039/d2sm01275h.

[37] Wittmar ASM, Koch D, Prymak O, Ulbricht M. Factors affecting the nonsolvent-induced phase separation of cellulose from ionic liquid-based solutions. ACS Omega 2020;5:27314–22. https://doi.org/10.1021/acsomega.0c03632.

[38] Goossens S, Goderis B, Groeninckx G. Reaction-induced phase separation in crystallizable micro- and nanostructured high melting thermoplastic/epoxy resin blends. Macromolecules 2006;39:2953–63. https://doi.org/10.1021/ma052742o.

[39] Wu HC, Nikzad S, Zhu C, Yan H, Li Y, Niu W, et al. Highly stretchable polymer semiconductor thin films with multi-modal energy dissipation and high relative stretchability. Nat Commun 2023;14. https://doi.org/10.1038/s41467-023-44099-w.

[40] Mun J, Ochiai Y, Wang W, Zheng Y, Zheng YQ, Wu HC, et al. A design strategy for high mobility stretchable polymer semiconductors. Nat Commun 2021;12. https://doi.org/10.1038/s41467-021-23798-2.

[41] Son SY, Lee G, Wang H, Samson S, Wei Q, Zhu Y, et al. Integrating charge mobility, stability and stretchability within conjugated polymer films for stretchable multifunctional sensors. Nat Commun 2022;13. https://doi.org/10.1038/s41467-022-30361-0.

[42] Mathew VS, Sinturel C, George SC, Thomas S. Epoxy resin/liquid natural rubber system: secondary phase separation and its impact on mechanical properties. J Mater Sci 2010;45:1769–81. https://doi.org/10.1007/s10853-009-4154-8.

[43] Kinloch AJ, Shaw SJ, Hunston DL. Deformation and fracture behaviour of a rubber-toughened epoxy: 2. Failure criteria. n.d.

[44] Ratna D. Phase separation in liquid rubber modi®ed epoxy mixture. Relationship between curing conditions, morphology and ultimate behavior. n.d.

[45] Yao K, Liu Z, Li T, Guo B, Zhuang Z. Mesoscale structure-based investigation of polyurea dynamic modulus and shock-wave dissipation. Polymer (Guildf) 2020;202. https://doi.org/10.1016/j.polymer.2020.122741.

[46] Montserrat S. Effect of crosslinking density on AC,(T,) in an epoxy network. vol. 36. 1995.

[47] Bellenger V, Verdu J, Morel E. Effect of structure on glass transition temperature of amine crosslinked epoxies. J Polym Sci B Polym Phys 1987;25:1219–34. https://doi.org/10.1002/polb.1987.090250604.